CHEMISTRY
AN ASIAN JOURNAL

www.chemasianj.org

A Journal of

ACES
Asian Chemical Editorial Society

REPRINT

WILEY-VCH

ACES Asian Chemical Editorial Society

DOI: 10.1002/asia.201701452

CHEMISTRY AN ASIAN JOURNAL Communication

Mesoporous Materials

Shape-Controlled Surface-Coating to Pd@Mesoporous Silica Core–Shell Nanocatalysts with High Catalytic Activity and Stability

Jie Ying,[a] Christoph Janiak,[c] Yu-Xuan Xiao,[a] Hao Wei,[a] Xiao-Yu Yang,*[a] and Bao-Lian Su*[a, b]

Abstract: Cubic Pd nanocrystals with shape-controlled mesoporous silica shells have been theoretically designed and successfully synthesized for investigating the effect of a porous nanoshell on catalytic performance of the core. Cubic Pd@cubic mesoporous silica keeps activity of all facets and shows highest catalytic activity and enhanced reusability in the hydrogenation of nitrobenzene.

Metal nanocrystals with unique electrical, optical, magnetic, and chemical properties have attracted enormous research interest in both fundamental studies and various practical applications.[1] However, due to the high surface energy of metal nanocrystals, aggregation often occurs with them, resulting in low stability and irregular morphologies, and limiting their applications, especially in catalysis. Surface nanocoating[2] is a universal and effective approach to stabilize nanocrystals and prevent leaching and/or severe particle agglomeration. Mesoporous silica, as an excellent candidate for shell nanoengineering, can not only endow the nanocrystals with high stability and large surface area, but also can facilitate the diffusion between the reactants and the products in catalytic reaction.[3] For example, Pt nanocrystals coated with a mesoporous silica shell reported by Somorjai et al. showed excellent catalytic activity and stability in high-temperature catalytic reactions.[4] Fe_2O_3 nanoparticles within a hierarchically macroporous core@ordered mesoporous shell synthesized by our group also exhibited high activity, high stability, and excellent recycling behaviour.[5] In such a nanoencapsulation technique, a better understanding of the micro/nano shell structures affecting the catalytic performance is of great importance to design high-performance nanocatalysts in terms of activity, selectivity and stability. Over the past few decades, the development of colloidal chemistry enabled nanometals to be readily prepared with tunable particle size, shape and composition.[6] The systematic investigations of these nanometals on catalytic properties have successfully been used to uncover atomic-scale characteristics, which are critical to catalytic activity and selectivity.[7] However, there is rarely an investigation on the shape of silica shells, although catalytic studies of nanometals within silica shell have shown the high thermal and chemical stabilities of such nanoparticle catalysts.[8] In this regard, the shape-controlled shell engineering is therefore highly demanded for fully understanding the effect of the nanoshell on catalytic performance.

Herein, we propose a rational design based on model calculation for fabrication of monodisperse cubic Pd nanocrystals with their shape-controlled mesoporous silica shells. Pd nanocubes embedded in three types of mesoporous silica with different shapes have been successfully synthesized: cubic Pd@cubic mesoporous silica, cubic Pd@thin spherical mesoporous silica, and cubic Pd@thick spherical mesoporous silica (denoted as Pd@$mSiO_2$-C, Pd@$mSiO_2$-S1 and Pd@$mSiO_2$-S2, respectively). We also carried out the hydrogenation of nitrobenzene to explore the catalytic activities of the cubic Pd without or with different shapes of mesoporous silica shells. The catalytic activities of all the samples show that the cubic silica shell can maximally retain the catalytic activity of the Pd core and greatly enhance the reusability compared to bare Pd.

The synthesis procedure for Pd@$mSiO_2$ core–shell nanostructures is illustrated in Figure 1. Firstly, cubic Pd nanocrystals were synthesized by using cetyltrimethyl ammonium bromide (CTAB) as the structure-directing agent and ascorbic acid (AA) as the reductant in an aqueous solution of H_2PdCl_4 at 95 °C. Then, a NaOH solution was added to the aqueous solution to adjust the pH of the solution to around 10–11, followed by adding a desired amount of tetraethyl orthosilicate (TEOS) to initiate the silica polymerization. After calcination of the as-synthesized Pd@$mSiO_2$ at 300 °C for 2 h, Pd@$mSiO_2$ nanoparticles were finally obtained. By adjusting the amount of TEOS, cubic Pd nanoparticles within three shapes of mesoporous silica shells were synthesized.

In order to rationally design the shapes of mesoporous silica shells, two regular models of cube@cube (model I; Figure 2a)

[a] Dr. J. Ying, Y.-X. Xiao, H. Wei, Prof. X.-Y. Yang, Prof. B.-L. Su
State Key Laboratory Advanced Technology for Materials Synthesis and Processing
Wuhan University of Technology
122, Luoshi Road, Wuhan, 430070 (China)
E-mail: xyyang@whut.edu.cn

[b] Prof. B.-L. Su
Laboratory of Inorganic Materials Chemistry (CMI)
University of Namur
61, rue de Bruxelles, 5000 Namur (Belgium)
E-mail: bao-lian.su@fundp.ac.be

[c] Prof. C. Janiak
Institut für Anorganische Chemie und Strukturchemie
Heinrich-Heine-Universität Düsseldorf
40204 Düsseldorf (Germany)

Supporting information and the ORCID identification number(s) for the author(s) of this article can be found under https://doi.org/10.1002/asia.201701452.

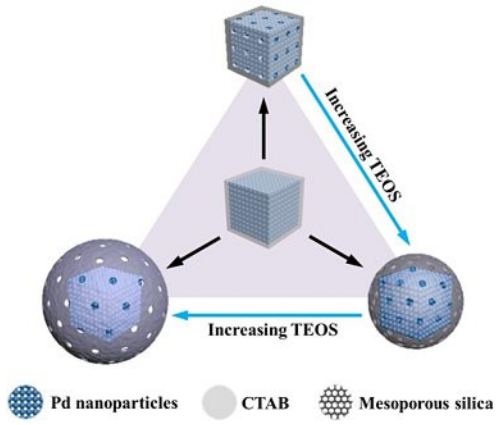

Figure 1. Schematic representation of the formation of Pd@mSiO$_2$ nanoparticles with different shapes.

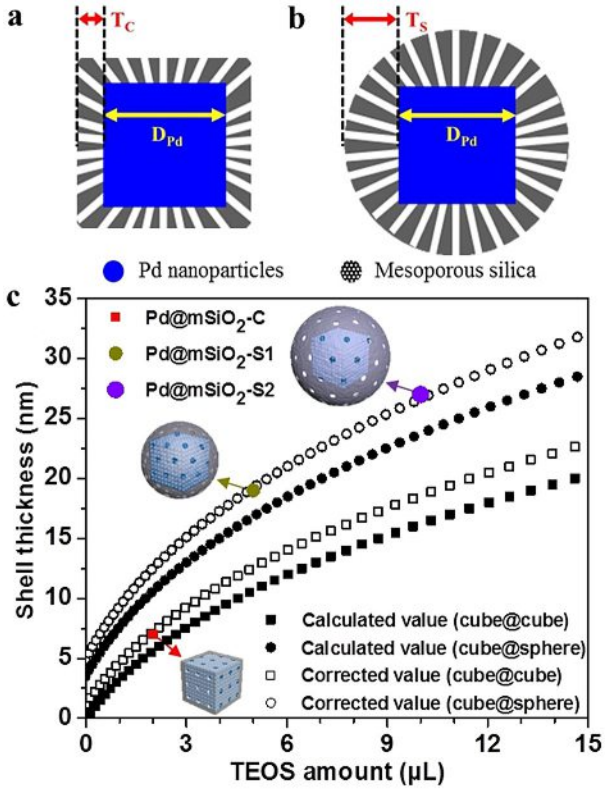

Figure 2. Schematic illustration of (a) cube@cube model and (b) cube@sphere model. (c) Calculation result of the relationship between TEOS volume and silica shell thickness of the synthesized Pd@mSiO$_2$ nanoparticle before (■ and ●) and after (□11$_2$ nanoparticles.

and cube@sphere (model II; Figure 2b) are proposed based on the epitaxial growth and minimum energy of silica, respectively. According to the models, the relationships between the TEOS volume (VTEOS; added pure TEOS volume) and silica thickness of the synthesized Pd@mSiO$_2$ nanoparticle with cubic shell (T_C; shown in Figure 2a) and spherical shell (T_S; shown in Figure 2b) are given by Equation (1) and (2), respectively (see the Supporting Information for details of the model calculation and calculated values in Figure 2c).

$$T_C = 15\sqrt[3]{0.793V_{TEOS} + 1} - 15 \quad (1)$$

$$T_S = 30\sqrt[3]{0.189V_{TEOS} + 0.239} - 15 \quad (2)$$

Notably, the silica thickness of the synthesized Pd@mSiO$_2$ nanoparticle can be easily tuned by the TEOS amount. To investigate their shape evolution, three different TEOS volumes of 2, 5 and 10 μL are chosen for the controlled synthesis of mesoporous silica shells. Scanning electron microscope (SEM) images show that the initially synthesized Pd nanocubes are uniform in size with an average particle diameter of 30(± 1.6) nm (Figure 3a,b and Figure S1). When adding a small

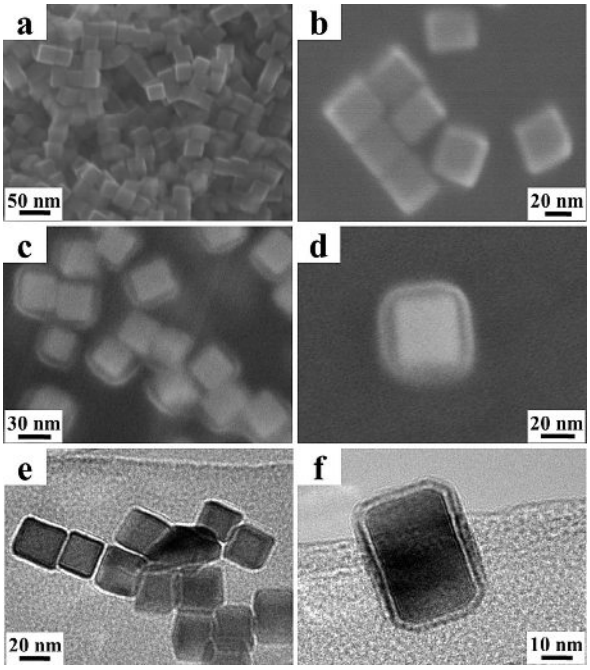

Figure 3. Representative low-resolution and high-resolution SEM images of Pd (a,b) and Pd@mSiO$_2$-C (c,d). Representative low-resolution and high-resolution TEM images of Pd@mSiO$_2$-C (e,f).

amount of TEOS (2 μL), Pd@mSiO$_2$-C consisting of a cubic Pd core and 7(± 1.2) nm-thick cubic silica shell was obtained (Figure 3c,d and Figure S2). Interestingly, the silica shell exhibits a cubic shape, which is very unique compared with usual spherical shape. The transmission electron microscopy (TEM) images (Figure 3e,f and Figure S3) further confirm this unique core–shell nanostructure with cubic core and cubic shell. This indicates that the silica was first formed on the surface of cubic Pd nanoparticles with an isotropic growth. When increasing the amount of TEOS (5 μL), Pd@mSiO$_2$-S1 with a thin spherical shell could be clearly observed (Figure S4a–c). The average thickness of silica shell of Pd@mSiO$_2$-S1 is 19(± 3.3) nm. The evolution toward a spherical shape is due to reduction of the surface-to-volume ratio.[9] Further increasing the amount of TEOS (10 μL), Pd@mSiO$_2$-S2 with a thick spherical shell could be obtained (Figure S4d–f), in accordance with the tendency

of the calculation result from model II. In view of the size of whole Pd@mSiO$_2$-S2, the average thickness of the mesoporous silica shell can also be calculated to be 27(±4.8) nm. Comparing with the calculated value based on corresponding model, the silica thicknesses of all Pd@mSiO$_2$ nanostructures are larger because of the unavoidable loss of Pd nanoparticles during the synthesis procedure and/or centrifuging/washing process. Therefore, to compensate the loss of Pd, it is necessary to introduce a correction coefficient (ε) to correct the total mass of Pd in Pd@mSiO$_2$. After correction, the relationships between V_{TEOS} and silica thickness with cubic shell (T'_C) and spherical shell (T'_S) are given by Equation (3) and (4), respectively (see Supporting Information for details of the correction).

$$T'_C = 15\sqrt[3]{0.793\varepsilon^{-1}V_{TEOS} + 1} - 15 \quad (3)$$

$$T'_S = 30\sqrt[3]{0.189\varepsilon^{-1}V_{TEOS} + 0.239} - 15 \quad (4)$$

Remarkably, as shown by corrected value in Figure 2c, the experimental silica thickness of all three types of the synthesized Pd@mSiO$_2$ can perfectly match with the corrected value of corresponding models when the set value of the ε is 0.93, which means that the unavoidable loss of Pd mass during synthesis should be 7%. These results demonstrate the validity and good guiding function of our model calculation.

Moreover, the crystallinity and porosity of Pd@mSiO$_2$ nanoparticles have also been measured. The high-angle X-ray diffraction (XRD) patterns (Figure S5) of Pd and Pd@mSiO$_2$ nanoparticles exhibit four similar and obvious peaks at 40.1°, 46.7°, 68.1°, and 82.1°, which can be assigned to (111), (200), (220), and (311) reflections of face-centered cubic (fcc) Pd (ICDD no. 05-0681). These peaks are broadened, indicating the nanoscale structural features. This result reveals that the crystal structure of Pd nanoparticles was maintained intact after the formation of the silica shell on cubic Pd. In particular, compared to bare Pd nanoparticles, the additional broad peaks around 23° in the XRD patterns of Pd@mSiO$_2$ nanoparticles can be ascribed to the silica.[10] The N_2 adsorption/desorption isotherms (Figure S6a) of all Pd@mSiO$_2$ nanoparticles exhibit a type II isotherm with a H3 hysteresis loop at high relative pressure, indicating their mesoporous characteristics. The pore sizes calculated using the Barrett-Joyner-Halenda (BJH) method (Figure S6b) of all types of Pd@mSiO$_2$ nanoparticles are around 3.5 nm with a narrow distribution. Due to the existence of the mesoporous silica shell, Pd@mSiO$_2$-C, Pd@mSiO$_2$-S1, and Pd@mSiO$_2$-S2 have high Brunauer-Emmett-Teller (BET) surface areas of 214 m^2g^{-1}, 296 m^2g^{-1}, and 364 m^2g^{-1}, respectively. The increase of the surface area can be attributed to the increase of the thickness and corresponding mesoporosity of these silica shells.

The above structural analyses confirm the formation of cubic Pd nanocrystals with shape-controlled mesoporous silica shells. Three shapes of mesoporous silica shells with cube, thin sphere, and thick sphere, have been successfully synthesized under the guidance of the model calculation. These cubic Pd with different shapes of mesoporous silica shells will help us to further investigate the effect of shape of mesoporous silica shell on catalytic performance, which has been rarely investigated previously. Therefore, we tested the catalytic activities of bare Pd and Pd@mSiO$_2$ nanoparticles for the hydrogenation of nitrobenzene, a model hydrogenation reaction, which the nitrobenzene can be converted into aniline by the catalysts under the hydrogen gas.

Figure 4a and Figure S7 show the conversion of nitrobenzene against time after adding the catalysts. As can be seen, the hydrogenation reaction rate is very fast, with 98.9% con-

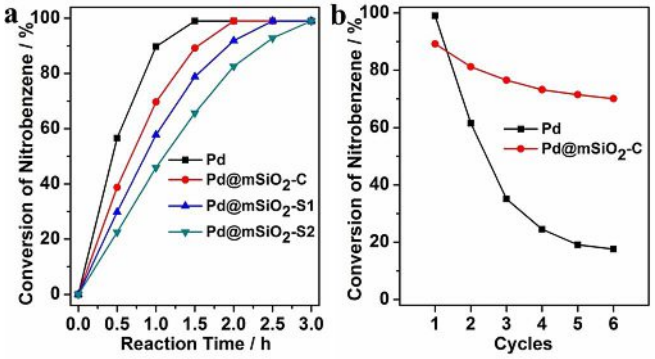

Figure 4. (a) The time-domain conversion of nitrobenzene by different catalysts of Pd, Pd@mSiO$_2$-C, Pd@mSiO$_2$-S1 and Pd@mSiO$_2$-S2 nanoparticles. (b) A comparison of conversion for Pd and Pd@mSiO$_2$-C nanoparticles during the six reaction cycles. The reaction time is 1.5 h.

version of nitrobenzene to aniline during 1.5 h after adding pure cubic Pd nanoparticles. Under the same catalytic conditions while substituting cubic Pd nanoparticles with same total amount of Pd in Pd@mSiO$_2$ nanocrystals, the conversions of nitrobenzene are 89.7%, 78.8% and 65.7% for Pd@mSiO$_2$-C, Pd@mSiO$_2$-S1 andPd@mSiO$_2$-S2, respectively (see the turnover frequency (TOF) values of all catalysts in Table S1). This catalysis result demonstrates that the catalytic activities of metal core are partly impeded by mesoporous silica shell, even though the reactant molecules and the product molecules can directly access to the Pd cores through the mesopores within the silica shells. The catalytic activity of Pd@mSiO$_2$-C is almost no change to that of the bare Pd, suggesting the cubic@cubic structure can keep the catalytic activity of all facets, and then retain the catalytic activity of metal core. Among all Pd@mSiO$_2$, Pd@mSiO$_2$-C shows the highest catalytic activity due to the thin silica shell and cubic-cubic structure, which not only be favour to diffusion of matters, but also helpful to exposure of active facets of cubic Pd. In addition, the catalytic activity of Pd@mSiO$_2$-C is also superior to that of the previously reported Pd-based catalysts (Table S2). To further investigate the effect of mesoporous shell on catalytic stability, we also did the reusability test of both bare Pd and Pd@mSiO$_2$-C. As shown in Figure 4b, Pd@mSiO$_2$-C shows far better reusability during the cycles of the hydrogenation of nitrobenzene reaction. There is only a slight decrease in the percent conversion between the reused and fresh Pd@mSiO$_2$-C after six cycles. In comparison,

an obvious decrease in activity is observed for bare cubic Pd. After six cycles of the hydrogenation of nitrobenzene reaction, Pd@mSiO$_2$-C retains 78.6% of the initial catalytic activity while only 17.8% of the initial catalytic activity is retained with bare cubic Pd. SEM measurements reveal that after six catalytic reaction cycles, Pd@mSiO$_2$-C largely maintained their morphologies while bare Pd showed severe ripening and aggregation (Figure S8). Overall, our studies demonstrate the greatly enhanced reusability of Pd@mSiO$_2$-C, which can be reasonably attributed to the protection of the mesoporous silica shell with a specific cubic shape.

In summary, we have rationally designed and successfully synthesized cubic Pd with three shapes of mesoporous silica shells: cube, thin sphere and thick sphere by adjusting the amount of silica sources based on model calculation. It is noted that cubic Pd with cubic mesoporous silica shell has been synthesized for the first time. These core–shell structured Pd@mSiO$_2$ nanoparticles with shape-controlled shell were used to investigate the effect of shape of mesoporous silica shell on catalytic performance of metal core. The catalysis results indicate that cubic mesoporous silica shell could maximally remain the catalytic activity of metal core and greatly enhance their reusability. Thus, it is believed that our method provides an effective approach to in-depth investigate the function of silica shell on metal core, and guide the rational design of this core–shell nanostructure for superior performance in catalysis.

Acknowledgements

This work was supported by the National Key R&D Program of China (2017YFC1103800), NSFC (U1663225, U1662134, 51472190, 51611530672, 51503166), ISTCP (2015DFE52870), PCSIRT (IRT_15R52) HPNSF (2016CFA033) and SKLPPC (PPC2016007), CNPC Research Institute of Safety and Environmental Technology.

Conflict of interest

The authors declare no conflict of interest.

Keywords: core–shell structures · heterogeneous catalysis · mesoporous materials · palladium · shape control

[1] a) J. Zecevic, G. Vanbutsele, K. P. de Jong, J. A. Martens, *Nature* **2015**, *528*, 245 – 248; b) K. Ding, A. Gulec, A. M. Johnson, N. M. Schweitzer, G. D. Stucky, L. D. Marks, P. C. Stair, *Science* **2015**, *350*, 189 – 192; c) Y. Zhou, D. Wang, Y. Li, *Chem. Commun.* **2014**, *50*, 6141 – 6144; d) W. C. Choy, *Chem. Commun.* **2014**, *50*, 11984 – 11993; e) L. Liu, U. Díaz, R. Arenal, G. Agostini, P. Concepción, A. Corma, *Nat. Mater.* **2017**, *16*, 132 – 138; f) D. Wang, H. L. Xin, R. Hovden, H. Wang, Y. Yu, D. A. Muller, F. J. DiSalvo, H. D. Abruña, *Nat. Mater.* **2013**, *12*, 81 – 87; g) X. Huang, Y. Li, Y. Chen, E. Zhou, Y. Xu, H. Zhou, X. Duan, Y. Huang, *Angew. Chem. Int. Ed.* **2013**, *52*, 2520 – 2524; *Angew. Chem.* **2013**, *125*, 2580 – 2584; h) X. Wang, H. Fu, A. Peng, T. Zhai, Y. Ma, F. Yuan, J. Yao, *Adv. Mater.* **2009**, *21*, 1636 – 1640; i) J. Ying, X.-Y. Yang, G. Tian, C. Janiak, B.-L. Su, *Nanoscale* **2014**, *6*, 13370 – 13382.

[2] a) W. Xia, R. Zou, L. An, D. Xia, S. Guo, *Energy Environ. Sci.* **2015**, *8*, 568 – 576; b) P. Wang, J. Zhao, X. Li, Y. Yang, Q. Yang, C. Li, *Chem. Commun.* **2013**, *49*, 3330 – 3332; c) J. Ying, X.-Y. Yang, Z.-Y. Hu, S.-C. Mu, C. Janiak, W. Geng, M. Pan, X. Ke, G. Van Tendeloo, B.-L. Su, *Nano Energy* **2014**, *8*, 214 – 222; d) J. Ying, Z.-Y. Hu, X.-Y. Yang, H. Wei, Y.-X. Xiao, C. Janiak, S.-C. Mu, G. Tian, M. Pan, G. Van Tendeloo, *Chem. Commun.* **2016**, *52*, 8219 – 8222; e) X. Y. Yang, Z. Q. Li, B. Liu, A. Klein-Hofmann, G. Tian, Y. F. Feng, Y. Ding, D. S. Su, F. S. Xiao, *Adv. Mater.* **2006**, *18*, 410 – 414; f) G. Yun, Z. Hassan, J. Lee, J. Kim, N. S. Lee, N. H. Kim, K. Baek, I. Hwang, C. G. Park, K. Kim, *Angew. Chem. Int. Ed.* **2014**, *53*, 6414 – 6418; *Angew. Chem.* **2014**, *126*, 6532 – 6536; g) K. Kojima, K. Chikama, M. Ishikawa, A. Tanaka, T. Nishikata, H. Tsutsumi, K. Igawa, H. Nagashima, *Chem. Commun.* **2012**, *48*, 10666 – 10668; h) B. Wu, D. Hu, Y. Yu, Y. Kuang, X. Zhang, J. Chen, *Chem. Commun.* **2010**, *46*, 7954 – 7956; i) J. Ying, G. Jiang, Z. P. Cano, L. Han, X. Y. Yang, Z. Chen, *Nano Energy* **2017**, *40*, 88 – 92; j) N. Yang, J. Liu, Y. Sun, Y. Zhu, *Nanoscale* **2017**, *9*, 2123 – 2128; k) J. Luo, F. He, S. Liu, *J. Porous Mater.* **2017**, *24*, 821 – 828; l) S. Cai, H. Hu, H. Li, L. Shi, D. Zhang, *Nanoscale* **2016**, *8*, 3588 – 3598.

[3] a) S. Liu, M. Y. Han, *Chem. Asian J.* **2010**, *5*, 36 – 45; b) J. Nakazawa, T. Hori, D. P. Stack, S. Hikichi, *Chem. Asian J.* **2013**, *8*, 1191 – 1199; c) Y. Fang, Y. Chen, X. Li, X. Zhou, J. Li, W. Tang, J. Huang, J. Jin, J. Ma, *J. Mol. Catal. A* **2014**, *392*, 16 – 21; d) Z. Li, H. C. Zeng, *J. Am. Chem. Soc.* **2014**, *136*, 5631 – 5639; e) J. Gao, X. Zhang, Y. Yang, J. Ke, X. Li, Y. Zhang, F. Tan, J. Chen, X. Quan, *Chem. Asian J.* **2013**, *8*, 934 – 938; f) C. Huo, J. Ouyang, H. Yang, *Sci. Rep.* **2014**, *4*, 3682; g) Y. Cao, M. Lu, J. Fang, L. Shi, D. Zhang, *Chem. Commun.* **2017**, *53*, 7549 – 7552.

[4] S. H. Joo, J. Y. Park, C.-K. Tsung, Y. Yamada, P. Yang, G. A. Somorjai, *Nat. Mater.* **2009**, *8*, 126 – 131.

[5] X. Y. Yang, Y. Li, G. Van Tendeloo, F. S. Xiao, B. L. Su, *Adv. Mater.* **2009**, *21*, 1368 – 1372.

[6] a) J. W. Hong, Y. Kim, Y. Kwon, S. W. Han, *Chem. Asian J.* **2016**, *11*, 2224 – 2239; b) D. B. Huang, P. L. He, Q. Yuan, X. Wang, *Chem. Asian J.* **2015**, *10*, 608 – 613; c) M. Cargnello, V. Doan-Nguyen, T. Gordon, R. Diaz, E. Stach, R. Gorte, P. Fornasiero, C. Murray, *Science* **2013**, *341*, 771 – 773; d) I. Do, L. Drzal, *Carbon* **2014**, *75*, 43 – 55; e) Y. Zheng, Y. Ma, J. Zeng, X. Zhong, M. Jin, Z. Y. Li, Y. Xia, *Chem. Asian J.* **2013**, *8*, 792 – 799; f) Q. L. Zhu, J. Li, Q. Xu, *J. Am. Chem. Soc.* **2013**, *135*, 10210 – 10213; g) S. Y. Liu, Y. T. Shen, C. Y. Chiu, S. Rej, P. H. Lin, Y. C. Tsao, M. H. Huang, *Langmuir* **2015**, *31*, 6538 – 6545.

[7] a) L. Zhang, L. T. Roling, X. Wang, M. Vara, M. Chi, J. Liu, S.-I. Choi, J. Park, J. A. Herron, Z. Xie, *Science* **2015**, *349*, 412 – 416; b) M. Li, Z. Zhao, T. Cheng, A. Fortunelli, C.-Y. Chen, R. Yu, Q. Zhang, L. Gu, B. Merinov, Z. Lin, *Science* **2016**, *354*, 1414 – 1419; c) L. Wang, Y. Yamauchi, *J. Am. Chem. Soc.* **2013**, *135*, 16762 – 16765; d) J. D. Padmos, M. L. Personick, Q. Tang, P. N. Duchesne, D.-e. Jiang, C. A. Mirkin, P. Zhang, *Nat. Commun.* **2015**, *6*, 7664; e) X. Huang, Y. Li, Y. Li, H. Zhou, X. Duan, Y. Huang, *Nano Lett.* **2012**, *12*, 4265 – 4270; f) E. Ye, M. D. Regulacio, S.-Y. Zhang, X. J. Loh, M.-Y. Han, *Chem. Soc. Rev.* **2015**, *44*, 6001 – 6017; g) N. Nalajala, W. F. G. Saleha, B. P. Ladewi, M. Neergat, *Chem. Commun.* **2014**, *50*, 9365 – 9368.

[8] a) J. M. Krier, W. D. Michalak, X. Cai, L. Carl, K. Komvopoulos, G. A. Somorjai, *Nano Lett.* **2015**, *15*, 39 – 44; b) Y. Hu, Y. Wang, Z.-H. Lu, X. Chen, L. Xiong, *Appl. Surf. Sci.* **2015**, *341*, 185 – 189; c) J. Lee, J. C. Park, H. Song, *Adv. Mater.* **2008**, *20*, 1523 – 1528; d) J. C. Park, H. J. Lee, J. Y. Kim, K. H. Park, H. Song, *J. Phys. Chem. C* **2010**, *114*, 6381 – 6388; e) X. Zhao, H. Li, J. Zhang, L. Shi, D. Zhang, *Int. J. Hydrogen Energy* **2016**, *41*, 2447 – 2456; f) X. Du, D. Zhang, R. Gao, L. Huang, L. Shi, J. Zhang, *Chem. Commun.* **2013**, *49*, 6770 – 6772.

[9] V. F. Puntes, K. M. Krishnan, A. P. Alivisatos, *Science* **2001**, *291*, 2115 – 2117.

[10] S. T. Selvan, T. Hayakawa, M. Nogami, Y. Kobayashi, L. M. Liz-Marzán, Y. Hamanaka, A. Nakamura, *J. Phys. Chem. B* **2002**, *106*, 10157 – 10162.

Manuscript received: October 9, 2017
Revised manuscript received: November 5, 2017
Accepted manuscript online: November 14, 2017
Version of record online: November 30, 2017